Supplementary Information

Simulation of the optimal diameter and wall thickness of hollow Fe_3O_4 microspheres in magnetorheological fluid

Lei Pei, Haoming Pang, Kaihui Chen, Shouhu Xuan* and Xinglong Gong*

CAS Key Laboratory of Mechanical Behavior and Design of Materials, Department of Modern Mechanics, University of Science and Technology of China, Hefei, Anhui, 230027, China.

E-mail: xuansh@ustc.edu.cn (S. Xuan); gongxl@ustc.edu.cn (X. Gong).

1. Non-linear curve fit of the magnetic hysteresis loop

The magnetic hysteresis loop of hollow Fe_3O_4 microspheres is described by using eqn (1) and the Langevin function respectively. In the rheological tests and applications of MR fluid, the magnetic field seldom exceeds 1 T. Only the curves between −10 kOe and 10 kOe are taken into consideration. In order to get a precise result, the modified Langevin function is adopted as:

$$M = M_0 + M_s\left[\coth\left(\frac{H-H_c}{s}\right) - \frac{s}{H-H_c}\right] \tag{S1}$$

Here M_s = 70.1 emu g^{-1}, H_c = 8.85 Oe, and s = 191.6 Oe. Both functions are in good agreement with experiments while eqn (1) is simpler.

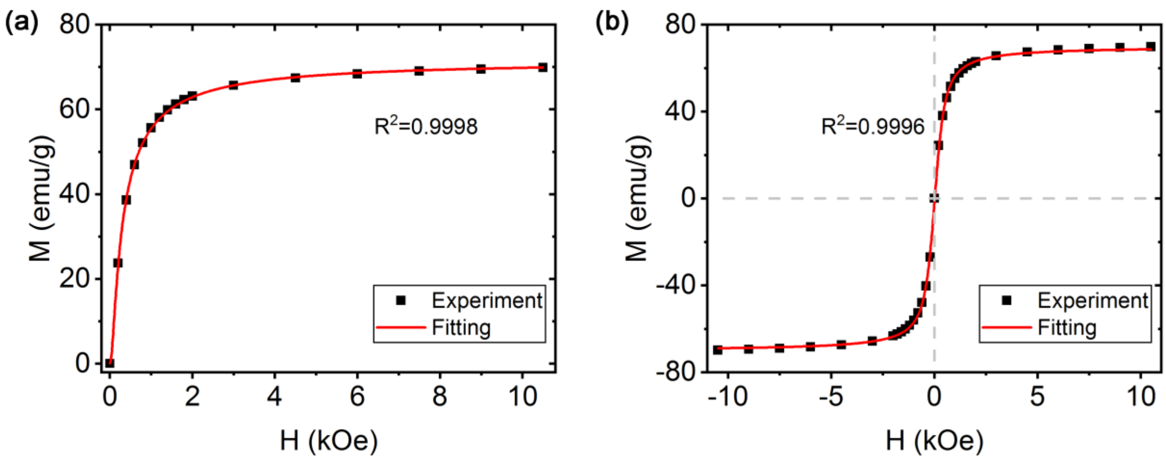

Fig. S1 Fitting curves by using (a) eqn (1) of the first quadrant and (b) eqn (S1) of the magnetic hysteresis loop between −10 kOe and 10 kOe.

2. Influence of the truncation radii

The truncation radius of magnetic force, van der Waals force, and excluded volume force varies from 3D – 8D, 1.5D – 4.0D, and 1.1D – 1.5D, respectively. D = 300 nm, H = 60 nm, B = 0.88 T, $\dot{\gamma}$ = 100 s^{-1}, and the weight fraction is set to 20 wt%. Small truncation radius for magnetic force and van der Waals force leads to a higher shear stress. If $r_{cm} \geq 5D$ $r_{cv} \geq 2.5D$ or $r_{cr} \geq 1.1D$, shear stress reaches a plateau. The excluded volume force increased exponentially with the decreasing r_{ij}. Proximal particles would exhibit a quite strong repulsive interaction. The situation of $r_{cr} < 1.1D$ was not considered. Therefore, the truncation radii in the main article are large enough to obtain accurate simulation results.

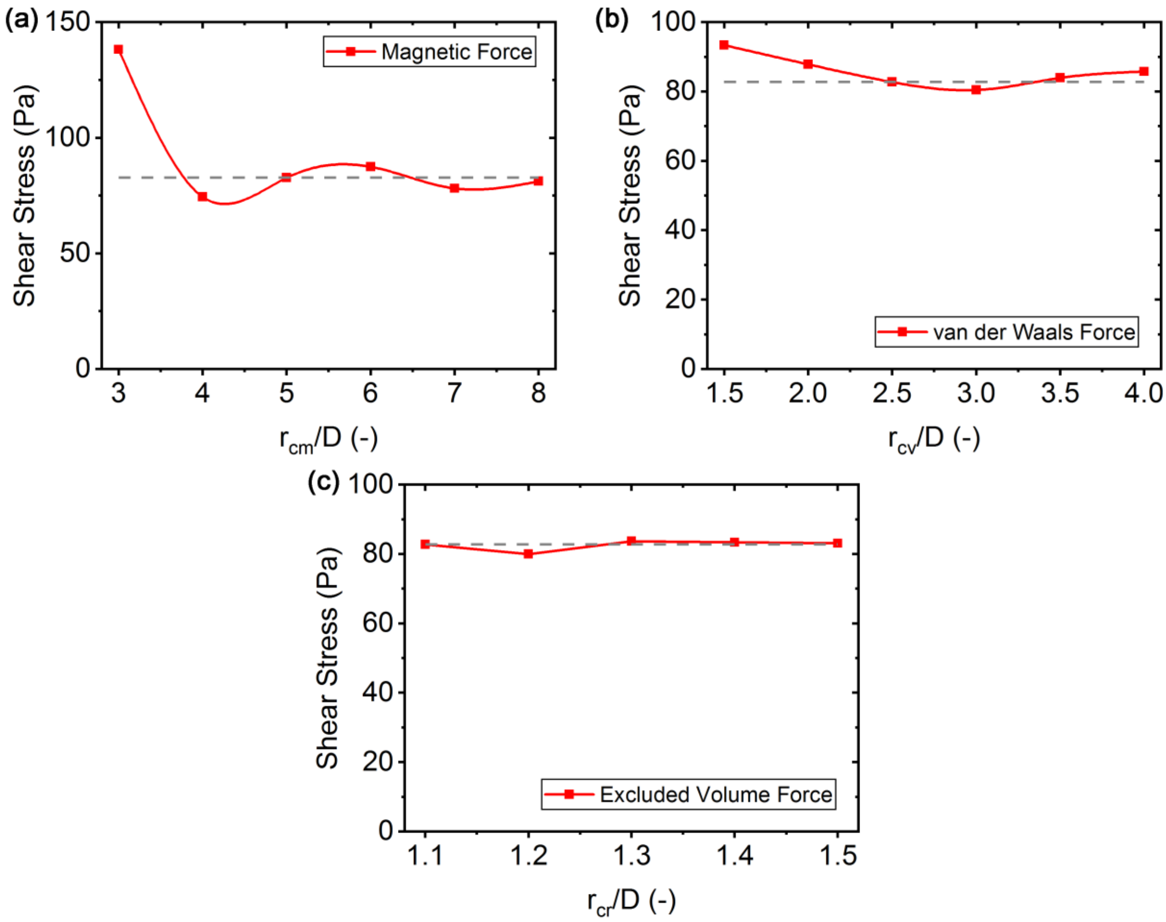

Fig. S2 Shear stress as a function of truncation radius for (a) magnetic force, (b) van der Waals force, and (c) excluded volume force. Dash lines represent the results under the same truncation radius as the main article.

3. Correction in hydrodynamic drag force

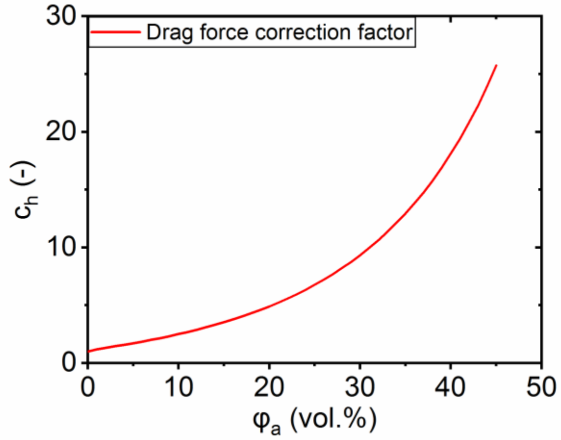

Fig. S3 Correctional factor c_h versus apparent volume fraction

The hydrodynamic drag force imposed on a particle grows faster as the local concentration increased. $c_h = 1$ at zero concentration, corresponding to an isolated particle. The drag force will become 8 times larger than isolation situation when the volume fraction reaches 30 vol.%. It is remarkable that hollow Fe_3O_4 microspheres with smaller wall thickness are subjected to larger hydrodynamic drag force due to their higher apparent volume fraction. Eqn (14) is obtained from an isotropic suspension. After applying the external magnetic field, MR fluid will form anisotropic microstructures. To our knowledge, investigation on the drag coefficient of anisotropic particle suspension with chain or lamellar microstructures has not been reported yet. In order to determine the drag force of Fe_3O_4 hollow microspheres, the simulation region should be large enough, for example, $L \geq 10D$. The local volume fraction of MR fluid under the external field is close to the overall apparent volume fraction when the truncation radius is $r_c > 5D$. Here the parameters D = 300 nm, H = 60 nm, B = 0.88 T, $\dot{\gamma}$ = 100 s^{-1}, and weight fraction 20 wt% are chosen as an example. Although the microstructures of MR fluid greatly change under the external field and shear flow, the apparent volume fraction approximately remains unchanged. Therefore, Eqn (14) is approximately adopted here.

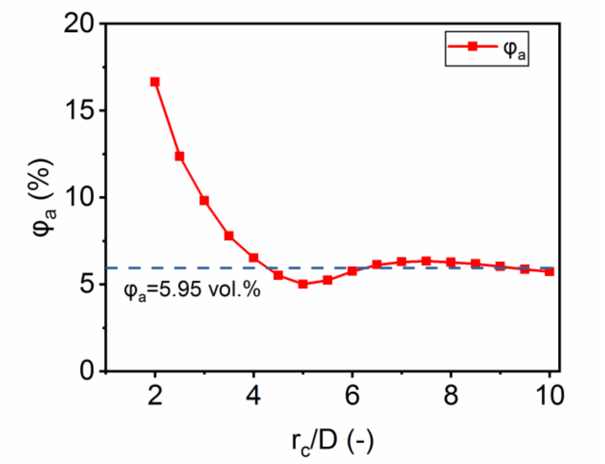

Fig. S4 Local volume fraction as a function of truncation radius. D = 300 nm, H = 60 nm, B = 0.88 T. Dash line represents the overall apparent volume fraction.

4. The intensity of particulate interactions as a function of the diameter

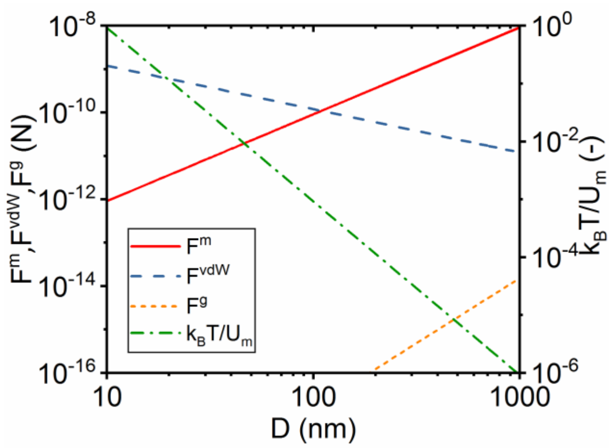

Fig. S5 The intensity of particle interactions versus diameter. Here two hollow spheres (H = 0.2D) were aligned in a head-to-tail configuration.

The magnetic energy is several orders of magnitude larger than thermal motion energy of the matrix. Brownian force becomes a match for magnetic force only when the diameter reduces to D = 10 nm. For the hollow microspheres in this study, the thermal motion energy of the matrix is much weaker than the magnetic energy between a pair of particles $k_B T \ll U_m$. If the diameter was 10 nm $\leq D \leq$ 100 nm, the van der Waals force between two proximal particles is stronger than the magnetic force. But the van der Waals force became much weaker if the diameter was $D \geq$ 200 nm. The gravity and buoyancy of magnetic particles $\boldsymbol{F}^g$ were always negligible.

The influence of Brownian force was also studied. The random force acting on each microsphere is described as:

$$\boldsymbol{F}_{\mathrm{B}}=\boldsymbol{R}\sqrt{\frac{6\pi k_{\mathrm{B}}TD\eta}{\delta t}} \tag{S2}$$

Where $\boldsymbol{R}$ is a unit random vector whose components are Gaussian numbers with zero mean. The time interval of Brownian force is chosen as $\delta t = 0.1\tau_{\mathrm{p}}$. $\tau_{\mathrm{p}} = D^2\rho_{\mathrm{p}}/18\eta$ is the characteristic time of microspheres and ρ_{p} is the density of microspheres. It is noted that the integral of this random force over a long time is independent on the choice of δt. In Fig. S6, hollow Fe_3O_4 microspheres with a wide range of diameters are chosen as examples. Here $B = 0.88$ T, $\dot{\gamma} = 100\ \mathrm{s}^{-1}$, and the weight fraction is 20 wt%.If the particle diameter changes from 100 nm to 1000 nm, τ_{p} will vary from 2×10^{-10} s to 10^{-8} s. Although this random force has a certain effect on the particle motion, the shear stress of the suspension only presented a small difference (<5%). In order to reduce the time consumption of the program, Brownian force is neglected in the equation of motion (eqn (17)).

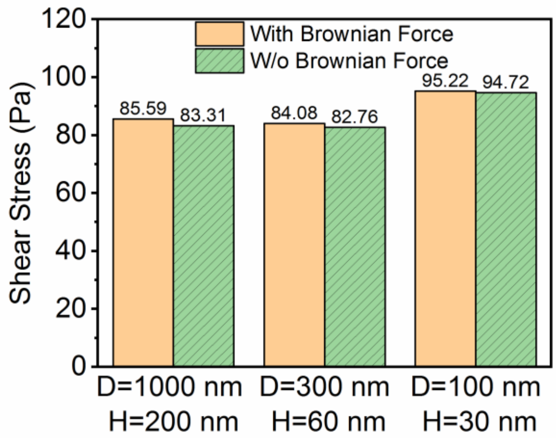

Fig. S6 Comparison between the simulated shear stress with Brownian force and without Brownian force.

5. Velocity-Verlet algorithm

The equation of motion is solved by using a modified velocity-Verlet algorithm.

$$\begin{cases} \boldsymbol{r}_i(t+\Delta t)=\boldsymbol{r}_i(t)+\boldsymbol{v}_i(t)\Delta t+1/2\,\boldsymbol{a}_i\Delta t^2 \\ \tilde{\boldsymbol{v}}_i(t+\Delta t)=\boldsymbol{v}_i(t)+\lambda\boldsymbol{a}_i(t)\Delta t \\ \boldsymbol{a}_i(t+\Delta t)=\boldsymbol{a}_i\left[\boldsymbol{r}_i(t+\Delta t),\tilde{\boldsymbol{v}}_i(t+\Delta t)\right] \\ \boldsymbol{v}_i(t+\Delta t)=\boldsymbol{v}_i(t)+1/2\left[\boldsymbol{a}_i(t)+\boldsymbol{a}_i(t+\Delta t)\right] \end{cases} \tag{S3}$$

Where $\tilde{\boldsymbol{v}}_i$ denotes the prediction of particle velocity at the next time step t+Δt. λ = 0.65 is an empirical parameter. The time step Δt adopted here is usually different from the time interval of Brownian force δt.

6. Influence of the orientation of particle chains to shear stress

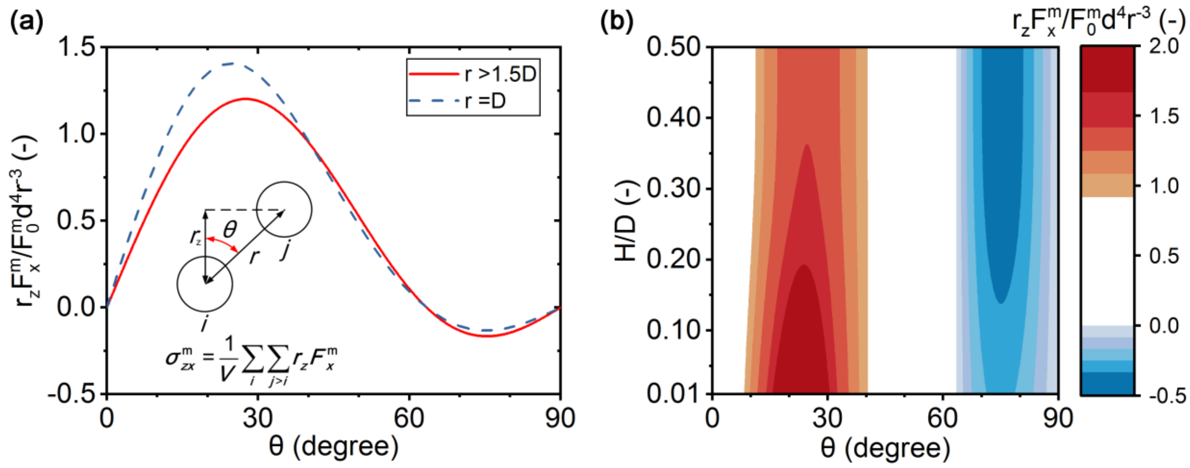

Fig. S7 The contribution of magnetic force to shear stress (a) as a function of inclined angle θ between two solid spheres; (b) as a function of *H*/*D* and inclined angle between two hollow spheres (*r* = *D*).

If the distance between two solid magnetic microspheres are fixed, the magneto-induced shear stress between them is dependent on θ. An inclined angle between 0 ° and 63.3 ° means a positive contribution to shear stress. The correction factor c_m in eqn (8) will enlarge this contribution. σ^m_{zx} achieves the maximum at 27.5 ° without the correction while at 24.7 ° with the correction. An inclined angle between 63.3 ° and 90 ° means a negative contribution. The σ^m_{zx} curve for $90° \leq \theta \leq 180°$ is antisymmetric with Fig. S7. When considering the superposition method in hollow microsphere system, both the maximum and minimum value of σ^m_{zx} decrease with the increasing wall thickness. The θ angle when σ^m_{zx} reaches the maximum also decreases for thin-walled microspheres.

7. Shear stress of 40 wt% hollow Fe_3O_4 MR fluid

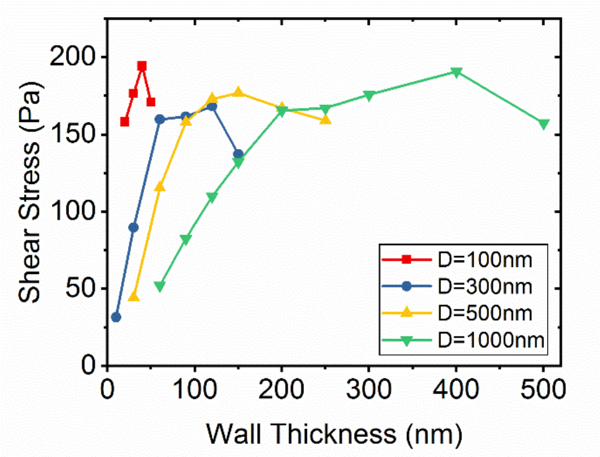

Fig. S8 Shear stress versus wall thickness curves from 40 wt% hollow Fe_3O_4 MR fluid.

The shear stress also firstly increased and then slightly decreased with the increasing wall thickness. If the wall thickness was fixed, the shear stress didn't monotonically decrease as the increasing diameter. Shear stress reached the maximum at *H* = 0.3*D* for *D* = 500 nm microspheres while at *H* = 0.4*D* for other microspheres. The peak value from those curves was 194 Pa, 168 Pa, 177 Pa, and 191 Pa, respectively.

8. Shear stress as a function of weight fraction

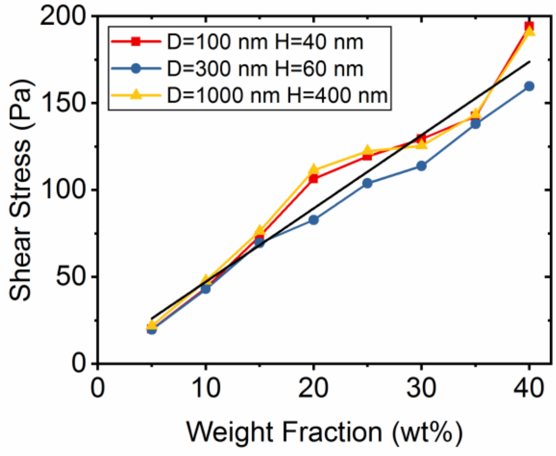

Fig. S9 Shear stress as a function of weight fraction.

The relationships between shear stress and weight fraction of hollow Fe_3O_4 microspheres is analyzed. Three kinds of microspheres: the two optimal architectures from simulation and the microspheres prepared in experiments are chosen as examples. Shear stress exhibits a linear dependence on the weight fraction (solid line in Fig. S9). In extreme dilute MR fluid (5 wt%), particle diameter and wall thickness only had weak effect on shear stress. When the weight fraction was less than 30 wt%, D = 1000 nm particles exhibited the advantage in MR effect. If the particle loading further increased, D = 100 nm particles presented the best shear stress. Shear stress expressed an accelerate growth when the weight fraction reached 40 wt%.